5-6-2014

Targeting Lactate Dehydrogenase-A Inhibits Tumorigenesis and Tumor Progression in Mouse Models of Lung Cancer and Impacts Tumor-Initiating Cells

Han Xie
Beth Israel Deaconess Medical Center

Jun-Ichi Hanai
Beth Israel Deaconess Medical Center

Jian-Guo Ren
Beth Israel Deaconess Medical Center

Lev Kats
Beth Israel Deaconess Medical Center

Kerri Burgess
Beth Israel Deaconess Medical Center

See next page for additional authors

Authors
Han Xie, Jun-Ichi Hanai, Jian-Guo Ren, Lev Kats, Kerri Burgess, Parul Bhargava, Sabina Signoretti, Julia Billiard, Kevin J. Duffy, Aaron Grant, Xiaoen Wang, Pawel Lorkiewicz, Sabrina Schatzman, Michael Bousamra, Andrew N. Lane, Richard M. Higashi, Teresa W-M Fan, Pier Paolo Pandolfi, Vikas P. Sukhatme, and Pankaj Seth

Targeting Lactate Dehydrogenase-A Inhibits Tumorigenesis and Tumor Progression in Mouse Models of Lung Cancer and Impacts Tumor-Initiating Cells

Notes/Citation Information
Published in *Cell Metabolism*, v. 19, no. 5, p. 795-809.

Digital Object Identifier (DOI)
http://dx.doi.org/10.1016/j.cmet.2014.03.003

Published in final edited form as:
Cell Metab. 2014 May 6; 19(5): 795–809. doi:10.1016/j.cmet.2014.03.003.

Targeting lactate dehydrogenase-A inhibits tumorigenesis and tumor progression in mouse models of lung cancer and impacts tumor initiating cells

Han Xie[1,&], **Jun-ichi Hanai**[1,&], **Jian-Guo Ren**[1,&], **Lev Kats**[3,&], **Kerri Burgess**[2,&], **Parul Bhargava**[5,&], **Sabina Signoretti**[5], **Julia Billiard**[6], **Kevin J. Duffy**[6], **Aaron Grant**[4,&], **Xiaoen Wang**[4,&], **Pawel K. Lorkiewicz**[7], **Sabrina Schatzman**[7], **Michael Bousamra II**[8], **Andrew N. Lane**[7,9], **Richard M. Higashi**[7,9], **Teresa W.M. Fan**[7,9,**], **Pier Paolo Pandolfi**[3,*,&], **Vikas P. Sukhatme**[1,2,*,&], and **Pankaj Seth**[1,*,&,π]

[1]Division of Interdisciplinary Medicine and Biotechnology, Beth Israel Deaconess Medical Center, Boston, Massachusetts 02215, USA

[2]Division of Hematology-Oncology, Beth Israel Deaconess Medical Center, Boston, Massachusetts 02215, USA

[3]Division of Genetics, Beth Israel Deaconess Medical Center, Boston, Massachusetts 02215, USA

[*]Department of Medicine, Beth Israel Deaconess Medical Center, Boston, Massachusetts 02215, USA

[&]Beth Israel Deaconess Cancer Center, Boston, Massachusetts 02215, USA

[4]Department of Radiology, Beth Israel Deaconess Medical Center and Harvard Medical School, Boston, Massachusetts 02215, USA

[5]Department of Pathology, Brigham and Women's Hospital and Harvard Medical School, Boston, Massachusetts 02215, USA

[6]Cancer Metabolism DPU, GlaxoSmithKline, Collegeville, Pennsylvania, 19426, USA

[7]Center for Regulatory & Environmental Analytical Metabolomics, Univ. of Louisville, Louisville, Kentucky 40208, USA

[8]Dept. Surgery, Univ. of Louisville, Louisville, Kentucky 40208, USA

[9]Graduate Center of Toxicology and Markey Cancer Center, 789 South Limestone St., University of Kentucky, Lexington, KY 40536 (ANL, TF, RMH present address)

[π]Address correspondence to: Pankaj Seth PhD, 330 Brookline Avenue, RW561, Boston MA 02215, Phone: 617-667-2029; Fax: 617-667-2110; pseth@bidmc.harvard.edu. [**]Co-corresponding Author: Teresa W.-M. Fan, PhD, Biopharm Complex, 789 South Limestone St., Lexington, KY 40536; Phone: 859-218-1028; Fax: 859-257-1307; teresa.fan@uky.edu.
J.H, J.G.R, L.K contributed equally to this study.

Summary

The lactate dehydrogenase-A (LDH-A) enzyme catalyzes the inter-conversion of pyruvate and lactate, is upregulated in human cancers and is associated with aggressive tumor outcomes. Here we use a novel inducible murine model and demonstrate that inactivation of *LDH-A* in mouse models of NSCLC driven by oncogenic *K-RAS* or *EGFR* leads to decreased tumorigenesis and disease regression in established tumors. We also show that abrogation of *LDH-A* results in reprogramming of pyruvate metabolism, with decreased lactic fermentation *in vitro, in vivo*, and *ex vivo*. This was accompanied by re-activation of mitochondrial function *in vitro* but not *in vivo* or *ex vivo*. Finally, using a specific small molecule LDH-A inhibitor, we demonstrated that *LDH-A* is essential for cancer initiating cell survival and proliferation. Thus, LDH-A can be a viable therapeutic target for NSCLC including cancer stem cell-dependent drug resistant tumors.

Introduction

The enhancement of aerobic glycolysis i.e. the Warburg effect (lactate production in the presence of adequate oxygen) (Warburg, 1930, 1956) not only provides cancer cells with a survival advantage, but also links it to invasive ability (Gatenby and Gillies, 2004). This effect has been seen in different types of tumors and the concomitant increase in glucose uptake is exploited clinically for detection of tumors by 2-fluorodeoxyglucose-based positron emission tomography (FDG-PET) (Gillies, 2001; Hsu and Sabatini, 2008).

Non-small cell lung cancer (NSCLC) is highly glycolytic, accounts for >85% of all lung cancers (Gazdar and Minna, 1999) and is the leading cause of cancer deaths. Mutations at codon 12, which constitute the majority of *K-RAS* mutations (Forbes et al., 2006) promote fermentative glycolysis in NSCLC (Vizan et al., 2005). Enhanced fermentative glycolysis in a hypoxic tumor microenvironment results in increased acid production (Ebert et al., 1996), which in turn lowers extracellular pH and has been linked to the metastatic ability of cancer cells (Fischer et al., 2007; Walenta et al., 1997).

K-RAS mutations have been frequently reported in NSCLC, particularly in adenocarcinoma (Riely et al., 2009). Mutations in *EGFR* are also common in NSC adenocarcinomas, and are generally exclusive with *K-RAS* mutations. Somatic activating mutations in *EGFR* produce a constitutively active tyrosine-kinase (L858R) and tumors bearing these mutations respond to the *EGFR* tyrosine kinase inhibitors (TKIs) gefitinib and erlotinib (Amann et al., 2005; Kobayashi et al., 2005). Clinically, despite the dramatic responses to such inhibitors, most patients relapse, owing to acquiring the resistance mutations (T790M, and L747S) (Costa et al., 2007). Any potential therapeutic opportunity that can address highly glycolytic NSCLC will have a significant clinical impact.

Tumor initiating cells (TICs) or cancer stem cells (CSCs) comprise a small population of tumor-forming, self-renewing, cancer cells within a tumor and are associated with aggressive disease and poor prognosis (Ailles and Weissman, 2007). It has been suggested that CSCs cluster in hypoxic niches, rely on fermentative glycolysis and have decreased mitochondrial respiration similar to progenitor cells during normal development (Hill et al.,

2009; Zhou et al.). Glycolysis is known to be indispensable for progenitor proliferation and biosynthesis (Agathocleous et al., 2012).

Targeting tumor metabolism via anti-glycolytic therapies may offer a therapeutic opportunity as it represents a key converging step for multiple deregulated signaling pathways in cancer cells. The lactate dehydrogenase-A gene (*LDH-A*), a target for HIF-1α and MYC, is of particular interest because it catalyzes the NADH-dependent reduction of pyruvate to lactate, a step essential for regenerating the NAD^+, which is needed for maintaining glycolysis and other metabolic activities. Enhanced expression of *LDH-A* has been associated with evolution of aggressive and metastatic cancers in a variety of tumor types (Koukourakis et al., 2005). Since therapies to address highly glycolytic NSCLC tumors are limited, development of *LDH-A* inhibitors may have a significant impact on this patient population.

Here, we detail the generation of a tamoxifen regulated cre-recombinase conditional mouse model of *LDH-A* deletion (Cre^{tm}-*LDH-*$A^{fl/fl}$). To investigate the role of *LDH-A* in NSCLC, we have used Ccsp-rtTA/(tetO)7-*K-RAS*4b^{G12D} bitransgenic mice (Fisher et al., 2001) and Ccsp-rtTA/(tetO)-*EGFR* L858R-T790M (Regales et al., 2007) to generate Cre^{tm}-*LDH-*$A^{fl/fl}$;Ccsp-rtTA/(tetO)7-*K-RAS*4b^{G12D} and Cre^{tm}-*LDH-*$A^{fl/fl}$;Ccsp-rtTA/(tetO)-*EGFR*-L858R-T790M respectively. These Cre^{tm}-*LDH-*$A^{fl/fl}$;Ccsp-rtTA/(tetO)7-*K-RAS*4b^{G12D} and Cre^{tm}-*LDH-*$A^{fl/fl}$;Ccsp-rtTA/(tetO)-*EGFR*-L858R-T790M mice serve as preclinical models in which tumors can be initiated in lung tissue by induction of mutant *K-RAS* or *EGFR*-L858R-T790M by doxycycline while *LDH-A* can be removed in all adult tissues including the lung. This model has enabled us to test the impact of *LDH-A* inhibition in established tumors. We show that *LDH-A* expression is required for the development of *K-RAS* dependent tumors. Importantly, we also show that blockade of *LDH-A* is therapeutically efficacious in established mutated *K-RAS* and *EGFR*-L858R-T790M dependent tumors. Indeed, established tumors regress with reduced *LDH-A*.

We have also examined the impact of *LDH-A* suppression on cancer metabolism *in vitro*. We have previously shown that *LDH-A* abrogation leads to increased production of reactive oxygen species (ROS) and apoptosis in cancer cells, likely the result of increased respiration (Xie et al., 2009). Here, using stable isotope tracers coupled with metabolomic analysis (stable isotope-resolved metabolomics or SIRM), we demonstrated that *LDH-A* suppression in cultured cancer cells enhances the Krebs cycle, oxygen consumption and mitochondrial ROS production (Seth et al., 2011). Moreover, using SIRM, we have investigated the metabolic effect of LDH-A attenuation *in vivo* in our new mouse model and *ex vivo* in freshly prepared human NSCLC tissue slices. Similar to the *in vitro* result, glycolytic production of ^{13}C-lactate from $^{13}C_6$-glucose was attenuated in *LDH-A* suppressed mouse lung tumors and LDH-A inhibitor-treated human tumor slices, but the Krebs cycle activity was not activated either *in vivo* or *ex vivo*.

It has been speculated that cancer stem cells exhibit the Warburg phenotype and may benefit from anti-glycolytic therapies. We demonstrate that oncogenic *K-RAS*–expressing cancer stem cells are highly susceptible to loss of *LDH-A* expression. We also validate these findings using an *LDH-A* specific inhibitor.

Results

Generation and characterization of Cre^{tm}-*LDH-A*$^{fl/fl}$ mice

Since *LDH-A* deletion is embryonic lethal (data not shown), we have generated conditional *LDH-A* transgenic mice controlled by tamoxifen-regulated cre-recombinase (Cre^{tm}) for inducible inactivation the *LDH-A* gene. The schematic (Figures S1 A–H) describes *LDH-A* gene inactivation.

Loss of *LDH-A* results in hemolytic anemia

Within 6 weeks of tamoxifen treatment, Cre^{tm}-*LDH-A*$^{fl/fl}$ mice but not *LDH-A*$^{fl/fl}$ developed severe but non lethal hemolytic anemia as evidenced by reduced numbers of red blood cells (RBCs) in the peripheral blood (Figure S2A). Blood smears stained with May-Grunwald-Giemsa marked polychromasia indicating release of early RBCs from the marrow in response to peripheral hemolysis (Figure S2C). The spleens of transgenic animals were greatly enlarged due to marked expansion of red pulp from hyperplastic erythroid precursors, and increased hemosiderin deposits characteristic of RBC phagocytosis were evident (Figures S2B, C). Flow cytometry analysis further confirmed the expansion of CD71^{+}Ter119^{+} immature erythroblasts in the bone marrow, spleen and peripheral blood of Cre^{tm}-*LDH-A*$^{fl/fl}$ animals (Figure S2D). Notably, tamoxifen-treated Cre^{tm}-*LDH-A*$^{fl/+}$ animals developed a partial phenotype (Figures S2A–D), as evident in both morphologic and flow-cytometric analyses, demonstrating that *LDH-A* is haplo-insufficient with respect to erythropoiesis.

Reduction in *LDH-A* protein levels results in decreased tumorigenesis in a *K-RAS* driven NSCLC model

In order to generate mice that have all the alleles, Cre^{tm}-*LDH-A*$^{fl/fl}$ mice were mated with Ccsp-rtTA/(tetO)7-*K-RAS*4b^{G12D} (hereafter referred to as *K-RAS*) to generate Cre^{tm}-*LDH-A*$^{fl/fl}$;Ccsp-rtTA/(tetO)7-*K-RAS*4b^{G12D} (homozygous for *LDH-A*, hereafter referred as Cre^{tm}-*LDH-A*$^{fl/fl}$; *K-RAS*) or Cre^{tm}-*LDH-A*$^{fl/+}$;Ccsp-rtTA/(tetO)7-*K-RAS*4b^{G12D} (heterozygous for *LDH-A*, hereafter referred to as Cre^{tm}-*LDH-A*$^{fl/+}$;*K-RAS*). In these mice, addition of doxycycline turns on the oncogenic *K-RAS* expression in a lung specific manner and intraperitoneal injection of tamoxifen turns off *LDH-A* expression in all the adult organs. Similarly, control *LDH-A*$^{fl/fl}$-Ccsp-rtTA/(tetO)7-*K-RAS*4b^{G12D} mice lacking the Cre^{tm} gene were generated (hereafter referred to as *LDH-A*$^{fl/fl}$;*K-RAS*).

To assess the role of *LDH-A* in the initiation of oncogenic *K-RAS* tumors, we took 5 week old Cre^{tm}-*LDH-A*$^{fl/fl}$;*K-RAS* and Cre^{tm}-*LDH-A*$^{fl/+}$;*K-RAS* mice and initiated doxycycline treatment for an additional two weeks to activate mutant *K-RAS* (Figure 1A). Following that, we initiated intraperitoneal tamoxifen injection (10 mg ml^{-1}) in corn oil every day for 5 days. We validated success of cre-recombination by RT-PCR analysis by assessing loss of exon 2 and sequencing the truncated *LDH-A* protein (Figures S1I–K). The control was the identical experiment where we injected corn oil as a vehicle with the same schedule.

As shown in Figure 1, reduced *LDH-A* expression resulted in significant reduction in tumor area, suggesting that fermentative glycolysis is a key bioenergetic pathway in oncogenic *K-*

RAS driven tumors. The data also show that deletion of just one allele of *LDH-A* results in substantial tumor reduction in this model (Figures 1B, C). The decreased expression of *LDH-A* in lung tumors was verified by western blot analysis. No changes were detected in *LDH-B* expression when *LDH-A* gene was deleted (Figures 1D, E). To validate the effects of *LDH-A* abrogation *in vivo*, a single Cre^{tm}-*LDH-*$A^{fl/fl}$;*K-RAS* mouse was imaged using proton MRI (Figure 1F) and hyperpolarized ^{13}C MRSI (Figures 3F–H) before and after inactivation of *LDH-A* by tamoxifen administration. As shown (Figures 1F–H), the solid lesions exhibited reductions in the lactate-to-pyruvate ratio levels in the tumor just 10 days after final tamoxifen treatment. For the larger lesion, the ratio fell from 0.47±0.01 to 0.37±0.05, while for the smaller lesion the ratio fell from 0.50±0.04 to 0.31±0.10. The spectra illustrating this reduction in the smaller lesion are shown (Figure 1H). Furthermore, abrogation of *LDH-A* in tumors led to decreased lactate levels, an increased NAD^+/NADH ratio, and increased pyruvate and isocitrate levels (Figure 1I), all consistent with decreased mitochondrial oxidation.

Cleaved caspase-3 immunohistochemical analysis (IHC) showed increased apoptosis in *K-RAS* driven tumors that have reduced *LDH-A* expression (Figure 1J). We also observed reduced disease in lungs of tamoxifen-treated Cre^{tm}-*LDH-*$A^{fl/fl}$;*K-RAS* mice using high resolution axial CT images of lung/chest (Figure 1K).

Reduction in *LDH-A* protein levels results in regression of established tumors in a *K-RAS* driven NSCLC model

To assess whether inhibition of *LDH-A* in an established tumor can impact tumor progression, five week old Cre^{tm}-*LDH-*$A^{fl/fl}$;*K-RAS* and Cre^{tm}-*LDH-*$A^{fl/+}$;*K-RAS* mice were maintained on a doxycycline diet for an additional 9 weeks. Following that, we initiated intraperitoneal tamoxifen injections (10 mg ml^{-1}) in corn oil every day for 5 days (Figure 2A).

Deletion of just one allele of *LDH-A* results in substantial tumor reduction in this GEM model (Figures 2B, C). The decreased expression of *LDH-A* in lung tumors was verified by western blot analysis and no changes were detected in LDH-B expression when *LDH-A* gene was deleted (Figure 2D). The degree of *LDH-A* attenuation is consistent with the homozygous and heterozygous knockdown. Furthermore, to quantify the response of *LDH-A* ablation on tumor growth in Cre^{tm}-*LDH-*$A^{fl/fl}$;*K-RAS* in real time, we scanned Cre^{tm}-*LDH-*$A^{fl/fl}$;*K-RAS* and *LDH-*$A^{fl/fl}$;*K-RAS* mice pre and the post-tamoxifen treatment. We observed marked regression in tumor growth 10 day post last tamoxifen treatment as measured by coronal and transverse section CT imaging (Figures 2F, G) and representative volumetric assessment of the total lung volume (Movie S1). These results suggest that targeting *LDH-A* in a *K-RAS* driven tumor results in tumor regression and targeting *LDH-A* in lung cancer might have therapeutic efficacy.

Reduction in *LDH-A* protein levels results in decreased tumorigenesis and regression of established tumors in *EGFR* resistant NSCLC model

It is possible that other aggressive lung tumors such as those that are resistant to *EGFR* inhibitors would be amenable to therapeutic targeting via *LDH-A*. To test this hypothesis, we

generated a Cre^{tm}-*LDH-A*$^{fl/fl}$;Ccsp-rtTA/(tetO)-*EGFR*-L858R-T790M mouse model (referred as Cre^{tm}-*LDH-A*$^{fl/fl}$;*EGFR*-T790M). These mice express *EGFR* mutation L858R as well as T790M mutation. Similar to the *K-RAS* model, the *EGFR*-L858R-T790M expression can be activated in lung epithelial cells by doxycycline and *LDH-A* expression (whole body) can be modulated by administering tamoxifen.

Five week old Cre^{tm}-*LDH-A*$^{fl/fl}$;*EGFR*-T790M, Cre^{tm}-*LDH-A*$^{fl/+}$;*EGFR*-T790M and *LDH-A*$^{fl/fl}$;*EGFR*-T790M mice were maintained on a doxycycline diet for additional 8 weeks, as shown (Figure 3A). The response of *LDH-A* suppression on tumor growth in Cre^{tm}-*LDH-A*$^{fl/+}$;*EGFR*-T790M was quantified in real time, we performed MRI scans of Cre^{tm}-*LDH-A*$^{fl/fl}$;*EGFR*-T790, Cre^{tm}-*LDH-A*$^{fl/+}$;*EGFR*-T790 and *LDH-A*$^{fl/fl}$;*EGFR*-T790 mice pre and post tamoxifen treatment. We show marked regression in tumor growth 20 days post after the last tamoxifen treatment as measured by coronal and transverse section imaging by CT scan (Figures 3B, C) and volumetric assessment of total lung volume. The graphical representation of volumetric analysis is shown as net change in lung volume (Figure 3E). The decreased expression of *LDH-A* in lung tumors was verified by western blot analysis (Figure 3D). The data also show that deletion of *LDH-A* results in substantial tumor reduction similar to the *K-RAS* model. These results suggest that targeting *LDH-A* in *EGFR*T-790M driven tumors results in tumor regression. However, unlike the *K-RAS* tumors where heterozygous ablation of *LDH-A* was therapeutically efficacious, the *EGFR*-T790M driven tumors showed a smaller decrease and 1 out of 4 tumors showed increase in tumor growth in the 4th week of monitoring.

Genetic and pharmacologic targeting of *LDH-A* suppress cancer stem cell function

We next asked whether CSCs are susceptible to reduction in *LDH-A* levels. To investigate the *in vivo* role of *LDH-A* in tumor initiating capacity in oncogenic *K-RAS* tumors, we isolated tumor cells from Cre^{tm}-*LDH-A*$^{fl/fl}$;*K-RAS* or Cre^{tm}-*LDH-A*$^{fl/fl}$;*K-RAS* mice that were treated with tamoxifen. As shown in Figure 4, when introduced via tail vein in C57BL6 mice, tumor cells with diminished *LDH-A* expression colonized the lung at a significantly decreased rate compared to tumor cells that have normal levels of *LDH-A* expression (Figure 4B). Injection of A549 cells expressing control or *LDH-A* shRNA in tail vein metastasis assay in athymic mice gave similar results (Figure 4A). Reduction in *LDH-A* expression in both A549 and Cre^{tm}-*LDH-A*$^{fl/fl}$;*K-RAS* was confirmed by western immunoblotting (Figures 4C, D). These findings are consistent with an *in vitro* matrigel invasion assay with NSCLC A549 cells expressing *LDH-A* shRNA (Figure 4C). Collectively these data suggest that blockade of fermentative glycolysis diminishes tumor initiating capacity, possibly via blocking cancer stem cells.

Next, to assess the role of *LDH-A* on CSCs *in vitro*, we next down-regulated *LDH-A* by shRNA in A549 cells and seeded them in a tumorsphere formation assay. As shown (Figures 4E, F), down-regulation of *LDH-A* expression significantly reduced the ability of A549 cells to form tumorspheres. To assess whether these results can be recapitulated in another oncogenic *RAS* cell line, we utilized a well-established *RAS* -induced mammary tumorigenesis system (HMLER) that has been used for CSCs analysis (Al-Hajj et al., 2003; Mani et al., 2008). We found that down regulation of *LDH-A* in this system results in a

significant decrease in CSCs as assessed by tumorsphere assay and by the expression of CD24/44 markers (Figure 4G). We further showed that tumor cells isolated from lungs of tamoxifen-treated Cre^{tm}-*LDH-A*$^{fl/fl}$;*K-RAS* mice formed significantly fewer tumorspheres than lung cells from *LDH-A*$^{fl/fl}$;*K-RAS* mice, suggesting that *LDH-A* abrogation impacts cancer stem cells *in vivo* (Figures 4H, I).

To validate these findings with *LDH-A* suppression, we used a specific inhibitor of *LDH-A* (Compound 1) developed at GlaxoSmithKline (Figure 5A). Compound 1 inhibited recombinant human *LDH-A* enzyme with an K_i = 4.8 ± 1.1 nM and showed ~10-fold selectivity over LDH-B (Figure 5B) and results in apoptosis (Billiard et al., 2013). Compound 1 decreased cellular lactate production in HepG2 hepatocellular carcinoma cells with an EC50 = 588 ± 200 nM (Figure 5C), increased ROS production (Figure 5D), decreased extracellular acidification rate (Figure 5E), and increased oxygen consumption rate (Figure 5F).

We also found that down regulation of *LDH-A* activity by Compound 1 reduced the ability of A549 cells to form tumorspheres (Figures 5G, H) and decreased the number of CD24/44 positive cells in HMLER system (Figure 5I) and in stem cells isolated from HMLER (Figure S5A). To investigate whether the observed decrease in CSCs is specific, we cultured HMLER cells with 10 μM Compound 1 for 48 hours before re-plating them in presence or absence of Compound 1. Figure 5J shows that CD24/44 positive cells re-appear after withdrawal of the inhibitor suggesting that Compound 1 affects CSC phenotype. Finally, treatment with Compound 1 significantly reduced the number of tumorspheres generated by tumor cells isolated from lungs of Ccsp-rtTA/(tetO)7-*K-RAS*4b^{G12D} mice (Figures 5K, L).

To investigate the specificity of *LDH-A* inhibitor targeting stem v/s. non-stem, we performed proliferation assay, which showed that the *LDH-A* inhibitor does not exclusively target stem cells, but the impact on stem cells is significant compared to non-stem cells (S. Figure 5B). To extend our results, we also used another previously published stem cell system i.e. MCF10A cells expressing shPTEN or over-expressing PIK3CA (Hanai et al., 2013) to demonstrate that an *LDH-A* inhibitor reduced the stem cell population as assessed by the tumorsphere assay (Figure 6C).

Abrogation of *LDH-A* results in reactivation of mitochondrial function in cancer cells *in vitro*

In order to test the hypothesis that reduction in aerobic glycolysis as a result of *LDH-A* abrogation leads to reactivation of mitochondrial metabolism, we performed $^{13}C_6$-glucose (Glu) and $^{13}C_5$,$^{15}N_2$-glutamine (Gln) tracer experiments with A549 cells expressing control shRNA or *LDH-A* shRNA. We found by GC-MS increased amounts of total and ^{13}C-enriched Krebs cycle metabolites (citrate, cis-aconitate, αKG, fumarate, malate, and aspartate) derived from either [U-^{13}C] glucose (Figure 6A) or [U-^{13}C]-glutamine, (Figure 6B). In particular, the increased synthesis of doubly ^{13}C labeled ($^{13}C_2$- or m2-) and quadruply ^{13}C labeled ($^{13}C_4$- or m4-) citrate from $^{13}C_6$-glucose in *LDH-A* suppressed cells reflect enhanced Krebs cycle activity through the first and second turns, respectively (cf. atom-resolved pathway tracing in Figure 6A). Increased flux through the Krebs cycle in these cells was also evidenced by the enhanced accumulation of the $^{13}C_4$-isotopologues of

citrate, fumarate and malate derived from fully labeled glutamine during the first turn of the cycle (cf. Figure 6B). In contrast, ^{13}C enrichment of Glu was substantially attenuated (e.g. $^{13}C_5{}^{15}N$-Glu or m6-Glu in Figure 6B) by *LDH-A* suppression in A549 cells grown with $^{13}C_5,^{15}N_2$-Gln. The GC-MS result was corroborated by the 1D HSQC NMR data, as shown (Figure S6), where the abundance of the ^{13}C-3/^{13}C-4-Glu and ^{13}C-4-Glu-glutathione isotopomers was lower in *LDH-A* suppressed than in control cells. Even more attenuated was the abundance of ^{13}C-4-Gln, which could be accounted for by decreased uptake and/or increased utilization of labeled Gln through the Krebs cycle; the latter is consistent with increased synthesis of labeled products of $^{13}C_5,^{15}N_2$-Gln oxidation through the Krebs cycle (cf. Figure 6B). We further noted that despite the reduction in levels of all ^{13}C labeled Glu isotopologues in *LDH-A* suppressed cells (Figure 6B), their fractional enrichment in these cells was comparable to that in control cells (Figure S6). The lack of change in ^{13}C fractional distribution together with decreased abundance of Glu and Gln is consistent with both reduced uptake of glutamine and increased glutaminolysis via the Krebs cycle induced by *LDH-A* knockdown. Enhanced pyruvate carboxylation observed could represent another anaplerotic path enhanced in *LDH-A* suppressed cells perhaps to compensate for the decreased Gln uptake. Overall decreased synthesis of glutathiones (reduced and oxidized forms) and increased mitochondrial metabolism is expected to lead to increased levels of ROS.

The above findings are in line with our hypothesis that ROS generated in response to *LDH-A* inhibition as a result of increased flux of pyruvate into the mitochondria. We have also demonstrated that these ROS are indeed mitochondrial in origin (data not shown). The static metabolic profiles from Cre^{tm}-*LDH-A*$^{fl/fl}$;*K-RAS* or Cre^{tm}-*LDH-A*$^{fl/+}$;*K-RAS* tumors (Figure 1I, H and Figure S3) corroborated the ^{13}C tracer analysis of increased Krebs cycle activity as well as reduced glutathione synthesis and increased NAD^+/NADH ratio in *LDH-A* suppressed cells.

Our mouse model provides a unique opportunity to investigate metabolic reprogramming in tumors *in vivo* in live animals via SIRM, using $^{13}C_6$ glucose as tracer in the Cre^{tm}-*LDH-A*$^{fl/fl}$;*K-RAS* and *LDH-A*$^{fl/fl}$;*K-RAS* mice post tamoxifen treatment. Figure 7A shows ^{13}C abundance data of lactate and other key metabolites in lung tumors derived from labeled glucose for 4 separate experiments. Relative to the control lung tumors (*LDH-A*$^{fl/fl}$;*K-RAS*), *LDH-A* suppressed lung tumor (Cre^{tm}-*LDH-A*$^{fl/fl}$;*K-RAS*) had reduced synthesis of ^{13}C-lactate (cf. ^{13}C-3-Lac) ($p<0.03$) which is consistent with reduced *LDH-A* activity. *LDH-A* knockdown lung tumors also led to reduced ^{13}C incorporation from labeled glucose into the Krebs cycle metabolites, including Asp, Glu, Gln, succinate, and citrate, although these effects did not reach statistical significance by Wilcoxon analysis (Figure 7, & Figure S4A). Nonetheless, this *in vivo* result contrasts with the enhanced Krebs cycle activity induced by *LDH-A* knockdown in cell culture (Figure 6). Metabolic distinctions between *in vivo* and *in vitro* systems have been observed for other tumors (Marin-Valencia et al., 2012), which could result from tumor micro-environmental factors absent in cell culture systems, including interaction with stromal cells and variable nutrient supply and oxygenation. Figure 7B shows the corresponding ^1H NMR spectra for one of the tumor pairs in Figure 7A. Unlabeled lactate (cf. H-3-Lac) and Ala (H-3-Ala) did not change while ^{13}C-Lac and Ala

(cf. $^{13}C_{sat}$-3 peaks) depleted with *LDH-A* knockdown. This result is consistent with reduced glycolytic flux from glucose to lactate, while lactate production from non-glucose sources may not have changed in response to *LDH-A* suppression.

To test how human lung tumor tissue metabolism responded to *LDH-A* attenuation, we employed *ex vivo* cancerous lung tissues freshly resected and thinly sliced from a human NSCLC patient (akin to "Warburg" slices). Similar tissue slices from other patients maintain metabolic activity (e.g. lactate and ATP synthesis) for up to 24 h under our culture conditions (data not shown). When tissue slices each were incubated with *LDH-A* inhibitor (Compound 1) + $^{13}C_6$-glucose or with inhibitor + $^{13}C_5$,$^{15}N_2$-glutamine for 24 h, ^{13}C-lactate production from labeled glucose (Figure 7C) was reduced while that from labeled glutamine was not (Figure 7D), which indicates a block in the *LDH-A* activity by the inhibitor without altering glutamine metabolism to lactate, corroborating with the *LDH-A* knockdown mouse tumor result described above (cf. Figure 7B). However, we noted reduced ^{13}C incorporation from labeled glutamine into the Krebs cycle metabolites such as succinate, citrate, and Asp (cf. Figure 7D) in response to *LDH-A* inhibition, which is consistent with the data obtained from *LDH-A* knockdown mice but deviates from the *in vitro* cell culture result (cf. Figure 6).

Discussion

This study allows us to reach a number of important conclusions: 1) reduced *LDH-A* expression in the adult mouse results in non-lethal anemia, but no other obvious toxicities; 2) reduced *LDH-A* expression in highly glycolytic tumors that expresses oncogenic *K-RAS* and/or *EGFR* L858R mutation in addition to resistant mutation T790M results in decreased tumorigenesis and regression of established tumors and as such may provide therapeutic benefit; 3) both homozygous and heterozygous deletion of *LDH-A* provides therapeutic efficacy; 4) *LDH-A* attenuation leads to reduced glycolytic flux *in vivo*, *ex vivo*, and *in vitro* but reactivation of the TCA cycle and anaplerosis occurs only *in vitro*, implicating the important role of the microenvironment in tumor metabolic reprogramming; 5) *LDH-A* inhibition impacts CSCs, a population of cells not targeted by most current therapies.

We show that loss of a single allele of *LDH-A* also results in decreased tumorigenesis. Therefore, it is likely that partial inhibition by a small molecule inhibitor directed against *LDH-A* may have potential anti-tumor activity. Of interest, we did not see compensation by increased expression of *LDH-B*, though we cannot rule out that the activity of this enzyme was not increased. These effects of *LDH-A* ablation on oncogenic *K-RAS* driven tumor growth were shared by tumors carrying *EGFR* L858R and T790M mutations, which render them insensitive to *EGFR* inhibitors.

Our data also show that *LDH-A* plays a critical role in tumor progression. Previous work from others and us has shown that that *LDH-A* suppressed cancer cell lines exhibit reduced tumor progression in xenograft models (Fan et al., 2011a; Fantin et al., 2006; Wang et al., 2011). These studies represent an important milestone in validating *LDH-A* as a therapeutic target, but they suffer from well-known artifacts of utilizing xenografts (Frese and Tuveson, 2007). Here we circumvented these issues by using a genetically engineered mouse (GEM) model. In this model, we temporally ablated *LDH-A* expression, enabling the investigation

of *LDH-A*'s role in tumor regression as well as in by-stander effect on non-tumor cells, which better approximates the use of a *LDH-A* inhibitor in a clinical setting. *LDH-A* ablation led to regression of an established tumor without serious systemic toxicity.

To our knowledge, this report is the first to show that abrogation of a metabolic enzyme in an established tumor model results in reduction of the tumor burden. In fact, metabolically targeted therapies generally delay tumor progression (Patra et al., 2013) or are cytostatic without causing regression (Bonnet et al., 2007; Hatzivassiliou et al., 2005).

In recent years, we have come to appreciate how substrate utilization is dictated by oncogenic enzymes (Nilsson et al., 2012). Based on our work, it is reasonable to hypothesize that all *RAS* transformed tumors and tumors with *EFGR* L858R mutations including those develop resistance to *EGFR* inhibitor therapy may respond to *LDH-A* inhibition.

By using labeled tracers and SIRM analysis, we were able to define metabolic reprogramming in lung tumor cells following *LDH-A* abrogation, i.e. increased flow of carbon from both glucose and glutamine through the Krebs cycle but reduced synthesis of glutathiones from glutamine. These reprogrammed events presumably underlie the enhanced oxygen consumption rate (OCR) and increased generation of ROS, previously observed by us (Xie et al., 2009). However, the mitochondrial perturbations in cultured tumor cells induced by *LDH-A* ablation was not recapitulated *in vivo* in our mouse model or *ex vivo* in human lung tumor slices, except for the reduced synthesis of glutathione's. Such discrepancies between *in vivo* and *in vitro* results have been observed in other tumor systems (e.g. glioma) (Marin-Valencia et al., 2012), and highlight the importance of tumor microenvironment and possibly systemic influence on tumor metabolic reprogramming, which in turns underlies inhibition of tumor growth or development.

Several publications described novel inhibitors of *LDH-A*, but most of the inhibitors are either inactive in cell based assays (Dragovich et al., 2013; Kohlmann et al., 2013) or have other problems (Le et al., 2010) as detailed in (Ward et al., 2012). The inhibitor used here (Billiard et al., 2013) is active in cell based assays at low μM concentrations in number of cell lines (Figure 5, and data not shown) and phenocopies the CSC results generated with either a cell line expressing *LDH-A* shRNA or tumors isolated from Cre^{tm}-*LDH-*$A^{fl/fl}$;*K-RAS* animals. Our attempts to use the *LDH-A* inhibitor for *in vivo* work, either in xenografts or GEMs, were limited by its pharmacokinetic properties.

Although it has been speculated that CSCs reside in hypoxic niche (Lock et al., 2013; Zhang et al., 2012) but relatively little is known about the metabolic properties of these cells. We show that reduced *LDH-A* expression impacts CSCs using established *in vivo*, *in vitro*, and *ex vivo* assays. Some of these findings were further validated with our novel *LDH-A* specific inhibitor. As in the case for non CSCs, these effects are likely to be mediated via perturbations to the mitochondrial Krebs cycle, as CSCs produce more ROS compared to non-stem counterpart. The ROS production by CSCs was further enhanced by *LDH-A* suppression (Figures S7A, B). Thus, CSCs could be more vulnerable to *LDH-A* blockade due to the overall lower capacity of their Krebs cycle (with limitation at the succinate dehydrogenase or SDH step of Complex II), despite a low glycolytic capacity, relative to the

non-CSCs (cf. Figure S7C). Complex II is prone to producing superoxide, and its over burden in *LDH-A* suppressed CSCs may account for the observed excess production of ROS. The Krebs cycle together with the electron transport chain would be less able to oxidize the excess pyruvate or regenerate NAD^+ in the cytoplasm via the malate/Asp shuttle to sustain glycolysis. The finding that *LDH-A* inhibition/ablation impacts cancer stem cells, a population of cells not targeted by a vast majority of current therapies, sets the stage for pre-clinical combinatorial trials with currently approved therapies for NSCLC.

Experimental Procedures

Cells and cell culture

A549 and HepG2 cells were purchased from the American Type Culture Collection and maintained in Ham's F-12 medium (Mediatech, Inc) with 10% FCS and penicillin/ streptomycin (P/S). Immortalized human breast epithelial cells (HMLE), were gifts from Dr. Weinberg (Whitehead Institute). All cell lines were grown as described earlier (Hanai et al., 2013).

Flow cytometry analysis and Fluorescence-Activated Cell Sorting (FACS)

HMLER cells were FACS-sorted into stem cell population (S: CD44 high and CD24 low) and non stem cell population (NS: CD44 low and CD24 high) as described earlier (Hanai et al., 2013).

Tumorsphere formation assay

Single cells were plated in 6-well ultra-low attachment plates (Corning) at a density of ~20,000 viable cells/ml and were processed as described earlier (Hanai et al., 2013). Two tailed *t* test was used to evaluate the statistical significance of the results. All values are expressed as mean ± S.E for this assay.

Oxygen consumption and PPR analysis by XF24 seahorse platform

The XF24 Extracellular Flux analyzer (Seahorse Biosciences, Billerica, MA) was used to measure oxygen consumption (OCR) and extracellular acidification rate (ECAR). Results were expressed as % ECAR or % OCR.

Steady State Metabolic analysis

Metabolic analysis was performed by BIDMC mass spectrometry core facility. Sample preparation was done according to a procedure developed by the core. Data were analyzed by the web server software located at http://www.metaboanalyst.ca/MetaboAnalyst/faces/Home.jsp. The normalized data were plotted using PRISM software.

Tamoxifen Treatment

All animal studies and procedures were approved by BIDMC Institutional Animal Care and Use Committee and were conducted in accordance with the BIDMC policy on the Care, Welfare and Treatment of Laboratory Animals. As described in the results section, the mice

were treated with tamoxifen (10 mg ml^{-1} in corn oil) or corn oil (only for fig. 3B) (Sigma) by intraperitoneal injection. A total of 76 mice were used in all the experiments.

Doxycycline Treatment

Doxycycline chow (Harlan, Teklad) was used as described previously (Fisher et al., 2001).

PCR genotype and western blot analysis

PCR primers developed by SANGER were used to detect modified *LDH-A* allele. Western blot analysis was carried out to further validate loss of *LDH-A* protein.

Statistical Analysis

Means, medians, Welch two tailed t-tests, Wilcoxon rank-sum test and descriptive-statistics were calculated as appropriate using Prism software package or Kaleidagraph (Synergy Software). The Error bars represented in each figure are mean +/− SD or +/− SEM and appropriate analysis is indicated in figure legends. P value $p< 0.05$ was considered statistically significant.

Tumor initiating cell assay

Athymic mice were injected via tail vein with either A549 cells (10^4 in 100μl) that were either expressing control shRNA or *LDH-A* shRNA. For tumor initiating cell assay in syngenic mice, tumor cells (10^4 in 100μl) isolated from either corn oil or tamoxifen treated Cre^{tm}-*LDH-A*$^{fl/fl}$;Ccsp-rtTA/(tetO)7-*K-RAS*4b^{G12D} mice were injected via tail vein. Animals were monitored for 21 days post injection and euthanized as per established guidelines. Total number of animals used for these assays were 20.

Tumor area measuring and Lung metastasis assay

Lung organs from 2mice bearing *RAS*-driven tumor were removed and washed three times with PBS. Formalin-fixed, paraffin-embedded mouse lung tissue sections were prepared at 5 μm. Each slide 2 or 3 sections cut from different distance were collected and stained by H&E method. H&E stained slides were scanned and tumor area were quantified with Image J (NIH software).

LDH enzymatic and Lactate production assay

These assays were performed as described earlier (Billiard et al., 2013).

Hyperpolarizer and proton imaging

All imaging procedures were approved by our Institutional Animal Care and Use Committee (IACUC) using methods described previously (Seth et al., 2011). ^{13}C magnetic resonance spectroscopic imaging (MRSI) was performed using two-dimensional chemical shift imaging (2D CSI) as described (Kohler et al., 2007).

Micro CT studies

Animals were anesthetized with 2% isoflurane/balance O2. Imaging was performed using the CT component of a NanoPET/CT (Bioscan, Washington, DC) scanner and image

analysis was performed using VivoQuant software (inviCRO, Boston, MA) using a Hounsfield Unit windowing technique, normalized for all scans. Volumetric segmentation was performed using a neighborhood threshold.

SIRM analysis

SIRM studies with ^{13}C-enriched tracers were carried out as previously described for both cells in culture and in mice (Fan et al., 2011b; Fan et al., 2012). Metabolites were analyzed by GC-MS and NMR according to standardized protocols as previously described (Lane et al., 2008), using in-house databases of standards for identification (Fan and Lane, 2008). Isotopomer distributions and fractional enrichments were calculated as previously described (Lane et al., 2008).

Warburg Slices

"Warburg slices" are thin slices (<1 mm thick) of tissue, two of which were immediately cut from a freshly resected human NSCLC tumor using a Weck microtome and were maintained in DMEM medium supplemented with 10% FBS, 1X penicillin and streptomycin plus 0.2% $^{13}C_6$-glucose and 2 mM glutamine or 0.2% glucose and 2 mM $^{13}C_5$,$^{15}N_2$-glutamine under 5% CO_2 at 37°C for 24 h without or with 20 μM Compound 1. The tissues were harvested by rinsing briefly in cold PBS, blotted dry and weighed before flash frozen in liquid N_2. Metabolites were extracted and analyzed by $^1H\{^{13}C\}$ HSQC NMR as described previously (Fan et al., 2011b; Fan et al., 2012).

Supplementary Material

Refer to Web version on PubMed Central for supplementary material.

Acknowledgments

This work was supported in part by Department of Defense award PC094151 (to P.S), grants for target award 2012-01-0602 (to P.S), NIH grants 5R01CA152330, 1R01GM098453 (to P.S), 1P01CA163223-01A1 (to A.N.L and T.F), 1U24DK097215-01A1 (to R.M.H, T.F, and A.N.L) and administrative supplement RM-11-024 (to P.S & T.F), R21EB01447 (to A.G) and startup funds from the Department of Medicine, BIDMC (to P.S). We would like to thank H. Varmus for providing the *K-RAS* animals, K. Wong for the *EGFR*-T790M mice, J. Tan and R. Balasubramaniam for processing the mouse and human tissue slice samples for SIRM analysis.

References

Agathocleous M, Love NK, Randlett O, Harris JJ, Liu J, Murray AJ, Harris WA. Metabolic differentiation in the embryonic retina. Nat Cell Biol. 2012; 14:859–864. [PubMed: 22750943]

Ailles LE, Weissman IL. Cancer stem cells in solid tumors. Curr Opin Biotechnol. 2007; 18:460–466. [PubMed: 18023337]

Al-Hajj M, Wicha MS, Benito-Hernandez A, Morrison SJ, Clarke MF. Prospective identification of tumorigenic breast cancer cells. Proc Natl Acad Sci U S A. 2003; 100:3983–3988. [PubMed: 12629218]

Amann J, Kalyankrishna S, Massion PP, Ohm JE, Girard L, Shigematsu H, Peyton M, Juroske D, Huang Y, Stuart Salmon J, et al. Aberrant epidermal growth factor receptor signaling and enhanced sensitivity to EGFR inhibitors in lung cancer. Cancer Res. 2005; 65:226–235. [PubMed: 15665299]

Billiard J, Dennison JB, Briand J, Annan RS, Chai D, Colon M, Dodson CS, Gilbert SA, Greshock J, Jing J, et al. Quinoline 3-sulfonamides inhibit lactate dehydrogenase A and reverse aerobic glycolysis in cancer cells. Cancer Metab. 2013; 1:19. [PubMed: 24280423]

Bonnet S, Archer SL, Allalunis-Turner J, Haromy A, Beaulieu C, Thompson R, Lee CT, Lopaschuk GD, Puttagunta L, Bonnet S, et al. A mitochondria-K+ channel axis is suppressed in cancer and its normalization promotes apoptosis and inhibits cancer growth. Cancer Cell. 2007; 11:37–51. [PubMed: 17222789]

Costa DB, Kobayashi S, Tenen DG, Huberman MS. Pooled analysis of the prospective trials of gefitinib monotherapy for EGFR-mutant non-small cell lung cancers. Lung Cancer. 2007; 58:95–103. [PubMed: 17610986]

Dragovich PS, Fauber BP, Corson LB, Ding CZ, Eigenbrot C, Ge H, Giannetti AM, Hunsaker T, Labadie S, Liu Y, et al. Identification of substituted 2-thio-6-oxo-1,6-dihydropyrimidines as inhibitors of human lactate dehydrogenase. Bioorg Med Chem Lett. 2013; 23:3186–3194. [PubMed: 23628333]

Ebert BL, Gleadle JM, O'Rourke JF, Bartlett SM, Poulton J, Ratcliffe PJ. Isoenzyme-specific regulation of genes involved in energy metabolism by hypoxia: similarities with the regulation of erythropoietin. Biochem J. 1996; 313(Pt 3):809–814. [PubMed: 8611159]

Fan J, Hitosugi T, Chung TW, Xie J, Ge Q, Gu TL, Polakiewicz RD, Chen GZ, Boggon TJ, Lonial S, et al. Tyrosine phosphorylation of lactate dehydrogenase A is important for NADH/NAD(+) redox homeostasis in cancer cells. Mol Cell Biol. 2011a; 31:4938–4950. [PubMed: 21969607]

Fan TW, Lane AN, Higashi RM, Yan J. Stable isotope resolved metabolomics of lung cancer in a SCID mouse model. Metabolomics. 2011b; 7:257–269. [PubMed: 21666826]

Fan TW, Lorkiewicz PK, Sellers K, Moseley HN, Higashi RM, Lane AN. Stable isotope-resolved metabolomics and applications for drug development. Pharmacol Ther. 2012; 133:366–391. [PubMed: 22212615]

Fan TWM, Lane AN. Structure-based profiling of Metabolites and Isotopomers by NMR. Progress in NMR Spectroscopy. 2008; 52:69–117.

Fantin VR, St-Pierre J, Leder P. Attenuation of LDH-A expression uncovers a link between glycolysis, mitochondrial physiology, and tumor maintenance. Cancer Cell. 2006; 9:425–434. [PubMed: 16766262]

Fischer K, Hoffmann P, Voelkl S, Meidenbauer N, Ammer J, Edinger M, Gottfried E, Schwarz S, Rothe G, Hoves S, et al. Inhibitory effect of tumor cell-derived lactic acid on human T cells. Blood. 2007; 109:3812–3819. [PubMed: 17255361]

Fisher GH, Wellen SL, Klimstra D, Lenczowski JM, Tichelaar JW, Lizak MJ, Whitsett JA, Koretsky A, Varmus HE. Induction and apoptotic regression of lung adenocarcinomas by regulation of a K-Ras transgene in the presence and absence of tumor suppressor genes. Genes Dev. 2001; 15:3249–3262. [PubMed: 11751631]

Forbes S, Clements J, Dawson E, Bamford S, Webb T, Dogan A, Flanagan A, Teague J, Wooster R, Futreal PA, et al. Cosmic 2005. Br J Cancer. 2006; 94:318–322. [PubMed: 16421597]

Frese KK, Tuveson DA. Maximizing mouse cancer models. Nat Rev Cancer. 2007; 7:645–658. [PubMed: 17687385]

Gatenby RA, Gillies RJ. Why do cancers have high aerobic glycolysis? Nat Rev Cancer. 2004; 4:891–899. [PubMed: 15516961]

Gazdar AF, Minna JD. Molecular detection of early lung cancer. J Natl Cancer Inst. 1999; 91:299–301. [PubMed: 10050857]

Gillies RJ. The tumour microenvironment: causes and consequences of hypoxia and acidity. Introduction. Novartis Found Symp. 2001; 240:1–6. [PubMed: 11727923]

Hanai JI, Doro N, Seth P, Sukhatme VP. ATP citrate lyase knockdown impacts cancer stem cells in vitro. Cell Death Dis. 2013; 4:e696. [PubMed: 23807225]

Hatzivassiliou G, Zhao F, Bauer DE, Andreadis C, Shaw AN, Dhanak D, Hingorani SR, Tuveson DA, Thompson CB. ATP citrate lyase inhibition can suppress tumor cell growth. Cancer Cell. 2005; 8:311–321. [PubMed: 16226706]

Hill RP, Marie-Egyptienne DT, Hedley DW. Cancer stem cells, hypoxia and metastasis. Semin Radiat Oncol. 2009; 19:106–111. [PubMed: 19249648]

Hsu PP, Sabatini DM. Cancer cell metabolism: Warburg and beyond. Cell. 2008; 134:703–707. [PubMed: 18775299]

Kobayashi S, Boggon TJ, Dayaram T, Janne PA, Kocher O, Meyerson M, Johnson BE, Eck MJ, Tenen DG, Halmos B. EGFR mutation and resistance of non-small-cell lung cancer to gefitinib. N Engl J Med. 2005; 352:786–792. [PubMed: 15728811]

Kohler S, Yen Y, Wolber J, Chen AP, Albers MJ, Bok R, Zhang V, Tropp J, Nelson S, Vigneron D, et al. In Vivo C13 Metabolic Imaging at 3T with Hyperpolarized C13-1-Pyruvate. Magn Reson Med. 2007; 58:65–69. [PubMed: 17659629]

Kohlmann A, Zech SG, Li F, Zhou T, Squillace RM, Commodore L, Greenfield MT, Lu X, Miller DP, Huang WS, et al. Fragment growing and linking lead to novel nanomolar lactate dehydrogenase inhibitors. J Med Chem. 2013; 56:1023–1040. [PubMed: 23302067]

Koukourakis MI, Giatromanolaki A, Simopoulos C, Polychronidis A, Sivridis E. Lactate dehydrogenase 5 (LDH5) relates to up-regulated hypoxia inducible factor pathway and metastasis in colorectal cancer. Clin Exp Metastasis. 2005; 22:25–30. [PubMed: 16132575]

Lane AN, Fan TW, Higashi RM. Isotopomer-based metabolomic analysis by NMR and mass spectrometry. Methods Cell Biol. 2008; 84:541–588. [PubMed: 17964943]

Le A, Cooper CR, Gouw AM, Dinavahi R, Maitra A, Deck LM, Royer RE, Vander Jagt DL, Semenza GL, Dang CV. Inhibition of lactate dehydrogenase A induces oxidative stress and inhibits tumor progression. Proc Natl Acad Sci U S A. 2010; 107:2037–2042. [PubMed: 20133848]

Lock FE, McDonald PC, Lou Y, Serrano I, Chafe SC, Ostlund C, Aparicio S, Winum JY, Supuran CT, Dedhar S. Targeting carbonic anhydrase IX depletes breast cancer stem cells within the hypoxic niche. Oncogene. 2013; 32:5210–5219. [PubMed: 23208505]

Mani SA, Guo W, Liao MJ, Eaton EN, Ayyanan A, Zhou AY, Brooks M, Reinhard F, Zhang CC, Shipitsin M, et al. The epithelial-mesenchymal transition generates cells with properties of stem cells. Cell. 2008; 133:704–715. [PubMed: 18485877]

Marin-Valencia I, Yang C, Mashimo T, Cho S, Baek H, Yang XL, Rajagopalan KN, Maddie M, Vemireddy V, Zhao Z, et al. Analysis of tumor metabolism reveals mitochondrial glucose oxidation in genetically diverse human glioblastomas in the mouse brain in vivo. Cell Metab. 2012; 15:827–837. [PubMed: 22682223]

Nilsson LM, Forshell TZ, Rimpi S, Kreutzer C, Pretsch W, Bornkamm GW, Nilsson JA. Mouse genetics suggests cell-context dependency for Myc-regulated metabolic enzymes during tumorigenesis. PLoS Genet. 2012; 8:e1002573. [PubMed: 22438825]

Patra KC, Wang Q, Bhaskar PT, Miller L, Wang Z, Wheaton W, Chandel N, Laakso M, Muller WJ, Allen EL, et al. Hexokinase 2 is required for tumor initiation and maintenance and its systemic deletion is therapeutic in mouse models of cancer. Cancer Cell. 2013; 24:213–228. [PubMed: 23911236]

Regales L, Balak MN, Gong Y, Politi K, Sawai A, Le C, Koutcher JA, Solit DB, Rosen N, Zakowski MF, et al. Development of new mouse lung tumor models expressing EGFR T790M mutants associated with clinical resistance to kinase inhibitors. PLoS One. 2007; 2:e810. [PubMed: 17726540]

Riely GJ, Marks J, Pao W. KRAS mutations in non-small cell lung cancer. Proc Am Thorac Soc. 2009; 6:201–205. [PubMed: 19349489]

Seth P, Grant A, Tang J, Vinogradov E, Wang X, Lenkinski R, Sukhatme VP. On-target inhibition of tumor fermentative glycolysis as visualized by hyperpolarized pyruvate. Neoplasia. 2011; 13:60–71. [PubMed: 21245941]

Vizan P, Boros LG, Figueras A, Capella G, Mangues R, Bassilian S, Lim S, Lee WN, Cascante M. K-ras codon-specific mutations produce distinctive metabolic phenotypes in NIH3T3 mice [corrected] fibroblasts. Cancer Res. 2005; 65:5512–5515. [PubMed: 15994921]

Walenta S, Salameh A, Lyng H, Evensen JF, Mitze M, Rofstad EK, Mueller-Klieser W. Correlation of high lactate levels in head and neck tumors with incidence of metastasis. Am J Pathol. 1997; 150:409–415. [PubMed: 9033256]

Wang ZY, Loo TY, Shen JG, Wang N, Wang DM, Yang DP, Mo SL, Guan XY, Chen JP. LDH-A silencing suppresses breast cancer tumorigenicity through induction of oxidative stress mediated mitochondrial pathway apoptosis. Breast Cancer Res Treat. 2011; 131:791–800. [PubMed: 21452021]

Warburg, o. The Metabolism of Tumors. London: Arnold Constable; 1930.

Warburg O. ORIGIN OF CANCER CELLS. Science. 1956; 123:309–314. [PubMed: 13298683]

Ward RA, Brassington C, Breeze AL, Caputo A, Critchlow S, Davies G, Goodwin L, Hassall G, Greenwood R, Holdgate GA, et al. Design and synthesis of novel lactate dehydrogenase A inhibitors by fragment-based lead generation. J Med Chem. 2012; 55:3285–3306. [PubMed: 22417091]

Xie H, Valera VA, Merino MJ, Amato AM, Signoretti S, Linehan WM, Sukhatme VP, Seth P. LDH-A inhibition, a therapeutic strategy for treatment of hereditary leiomyomatosis and renal cell cancer. Mol Cancer Ther. 2009; 8:626–635. [PubMed: 19276158]

Zhang Y, Zhang X, Wang X, Gan L, Yu G, Chen Y, Liu K, Li P, Pan J, Wang J, et al. Inhibition of LDH-A by lentivirus-mediated small interfering RNA suppresses intestinal-type gastric cancer tumorigenicity through the downregulation of Oct4. Cancer Lett. 2012; 321:45–54. [PubMed: 22429998]

Zhou W, Choi M, Margineantu D, Margaretha L, Hesson J, Cavanaugh C, Blau CA, Horwitz MS, Hockenbery D, Ware C, et al. HIF1alpha induced switch from bivalent to exclusively glycolytic metabolism during ESC-to-EpiSC/hESC transition. EMBO J. 31:2103–2116. [PubMed: 22446391]

Highlights

- An inducible *LDH-A* mouse model has been developed and characterized.
- Reduced *LDH-A* results in regression of established tumors in NSCLC mouse models.
- Cancer initiating cells are susceptible to *LDH-A* inhibition.
- Pharmacologic inhibition of LDH-A mimics the effects of genetic attenuation.

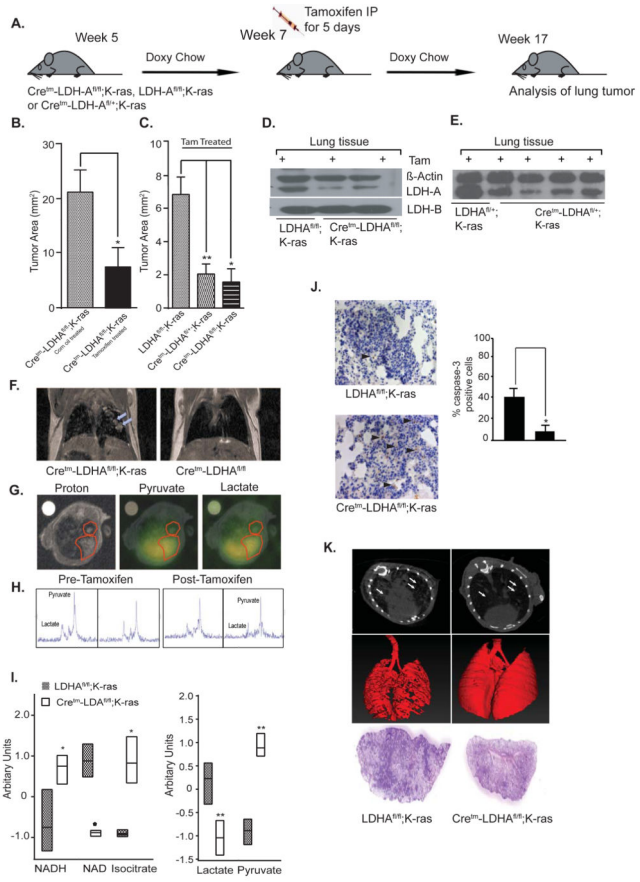

Fig. 1. *LDH-A* expression is required for initiation of oncogenic *K-RAS*-induced tumorigenesis

(**A**) Schematic representation of an experiment where *LDH-A* knockdown was initiated 14 days after *K-RAS* induction by doxycycline diet. (**B**) Tumor areas of Cre^{tm}-*LDH-A*$^{fl/fl}$;*K-RAS* mice treated with tamoxifen (n=7) or corn oil (n=6). (**C**) Tumor areas of Cre^{tm}-*LDH-A*$^{fl/fl}$;*K-RAS* (n=3), Cre$^{\mathbf{tm}}$-*LDH-A*$^{fl/+}$;*K-RAS* (n=5) and *LDH-A*$^{fl/fl}$;*K-RAS* (Cre^{tm} negative) mice (n=4) treated with tamoxifen (data in B and C are represented as mean ± SD, *= p < 0.05, **= p <0.01 as calculated by two tailed t test). (**D**) Representative western blot analysis of tumor (along with non-malignant cells) for *LDH-A*, LDH-B, and beta-actin from *LDH-A*$^{fl/fl}$;*K-RAS* and Cre^{tm}-*LDH-A*$^{fl/fl}$;*K-RAS* mice. (**E**) Representative western blot analysis of tumor (along with non-malignant cells) for *LDH-A*, and beta-actin from *LDH-A*$^{fl/fl}$;*K-RAS* and Cre^{tm}-*LDH-A*$^{fl/+}$;*K-RAS* mice (**F**) Coronal proton density weight images showing comparison of lungs in Cre^{tm}-*LDH-A*$^{fl/fl}$;*K-RAS* mouse on doxycycline diet (left) and Cre^{tm}-*LDH-A*$^{fl/fl}$ mouse (right). Tumors are indicated by arrows in image on left. (**G**) Proton (left), pyruvate (center), and lactate (right) images acquired in Cre^{tm}-*LDH-A*$^{fl/fl}$;*K-RAS* mice prior to tamoxifen administration. Red outlines are drawn around lung lesions. (**H**) Spectra acquired before (two left panels) and after (two right panels) tamoxifen withdrawal, with signals from pyruvate (pyr) and lactate (lac) labeled at left. (**I**) Metabolic profiling analysis of NADH, NAD$^+$, isocitrate, lactate, and pyruvate from *LDH-A*$^{fl/fl}$;*K-RAS* v/s. Cre^{tm}-*LDH-A*$^{fl/fl}$;*K-RAS* (see Fig. S3 for other pathway specific metabolites). (**J**) Representative caspase-3 staining of tumors from Cre^{tm}-*LDH-A*$^{fl/fl}$;*K-RAS* (top panel), and

LDH-A$^{fl/fl}$;*K-RAS* (bottom panel); quantitation of caspase 3 staining is shown on the right (means ± SD of n= 4 mice each). (**K**) Axial CT images and anterior/posterior (A/P) reconstruction from chest/lung and H&E staining of a lung section from *LDH-A*$^{fl/fl}$;*K-RAS* (left panel) and Cre^{tm}-*LDH-A*$^{fl/fl}$;*K-RAS* treated with tamoxifen (right panel).

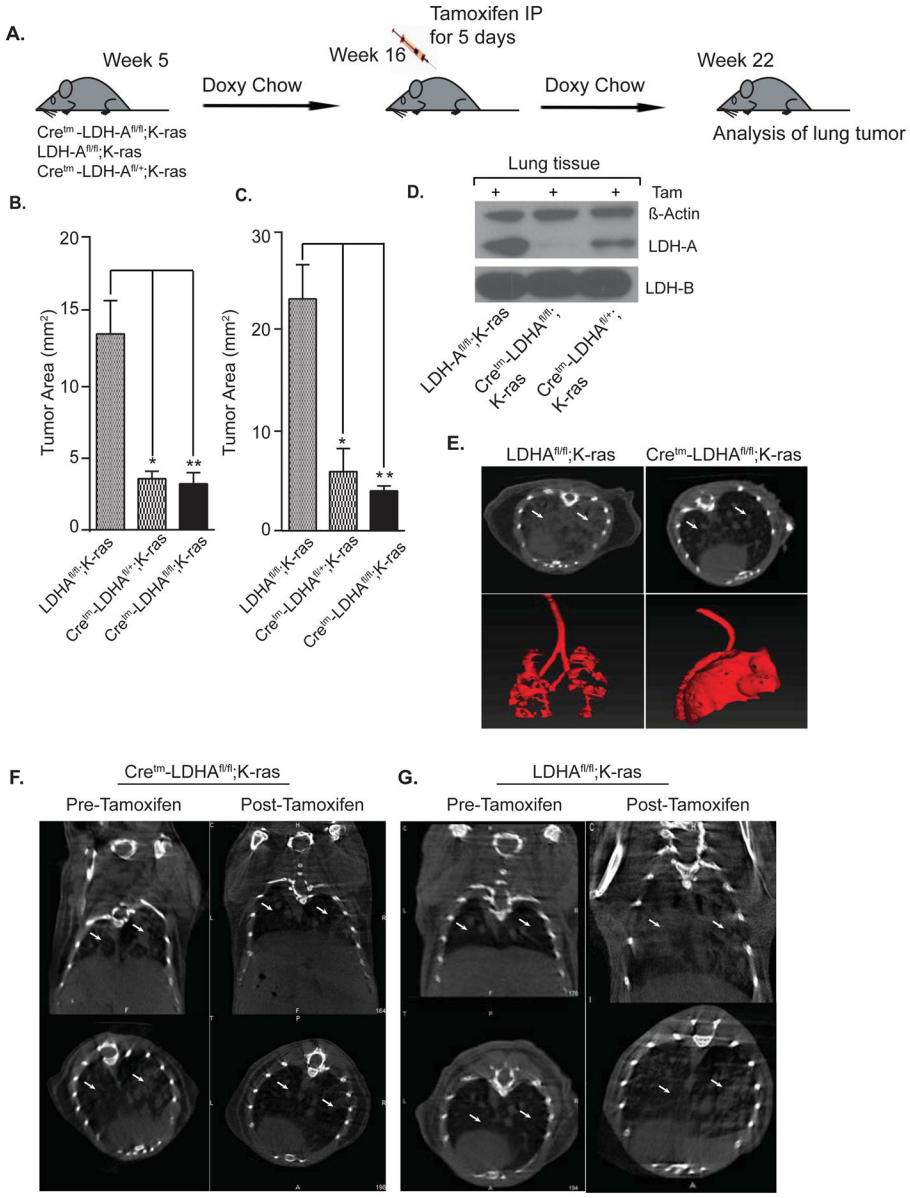

Fig. 2. Reduction in *LDH-A* levels results in reduced tumorigenesis of established tumors in a *K-RAS*-driven NSCLC model

(A) Schematic representation of an experiment where *LDH-A* knockdown was initiated ~83 days after *K-RAS* induction by doxycycline diet. (**B** & **C**) Tumor areas of Cre^{tm}-*LDH-A*$^{fl/fl}$;*K-RAS* (n=12), Cre^{tm}-*LDH-A*$^{fl/+}$;*K-RAS* (n=7), and *LDH-A*$^{fl/fl}$;*K-RAS* (n=6) mice that were treated with tamoxifen. Data is representated as mean ± SD, **=p, 0.01, *= p < 0.05 (two tailed t test) (**D**) Representative western blot analysis of tumors (along with non-malignant cells) from *LDH-A*$^{fl/fl}$;*K-RAS*, Cre^{tm}-*LDH-A*$^{fl/+}$;*K-RAS*, and Cre^{tm}-*LDH-A*$^{fl/fl}$;*K-RAS* mice for *LDH-A*, LDH-B, and beta-actin. (**E**) Axial CT images and anterior/posterior (A/P) reconstruction from chest/lung from *LDH-A*$^{fl/fl}$;*K-RAS* mice (left panel) and Cre^{tm}-*LDH-A*$^{fl/fl}$;*K-RAS* mice treated with tamoxifen (right panel) with tumors indicated by arrows (**F**) Representative coronal and transverse images of lung/chest from same pre and post

tamoxifen treated Cre^{tm}-*LDH-A*$^{fl/fl}$;*K-RAS* mice (n=5) in comparison to *LDH-A*$^{fl/fl}$;*K-RAS* mice (n=3).

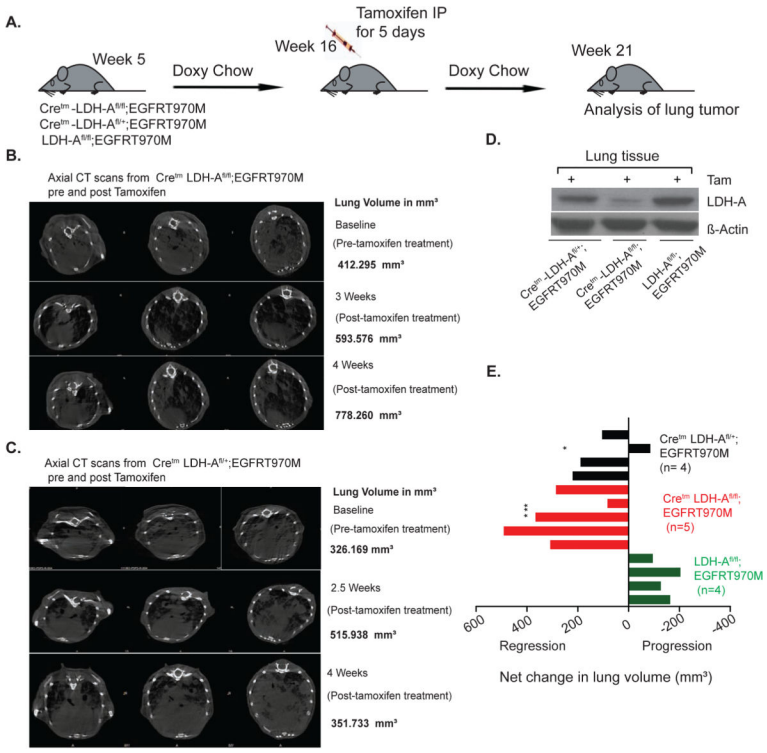

Fig. 3. Reduction in *LDH-A* levels results in reduced tumorigenesis of established tumors in *EGFR*- L858R-T970M driven NSCLC model

(A) Schematic representation of an experiment where *LDH-A* knockdown was initiated ~80 days after *EGFR*-T970M mutation induction by doxycycline diet. (**B** & **C**) Representative axial CT scans from pre and post Tamoxifen tumor volume of Cre^{tm}-*LDH-A*$^{fl/fl}$;*EGFR*-T970M, Cre^{tm}-*LDH-A*$^{fl/+}$;*EGFR*-T970M mice. (**D**) Representative western blot analysis of tumors (along with non-malignant cells) from *LDH-A*$^{fl/fl}$;*K-RAS*, Cre^{tm}-*LDH-A*$^{fl/+}$;*K-RAS*, and Cre^{tm}-*LDH-A*$^{fl/fl}$;*K-RAS* mice for *LDH-A*, and beta-actin. (**E**) Graphical representation of volumetric changes in lung volume pre and post tamoxifen Cre^{tm}-*LDH-A*$^{fl/fl}$;*EGFR*-T970M (n=5), Cre^{tm}-*LDH-A*$^{fl/+}$; *EGFR*T-970M (n=4), and *LDH-A*$^{fl/fl}$; *EGFR*T970M (n=4) mice that were treated with tamoxifen. Statistical data values are significant as tested by Dunnett's multiple comparisons test between all three genotypes (* WT to heterozygous and *** WT to homozygous).

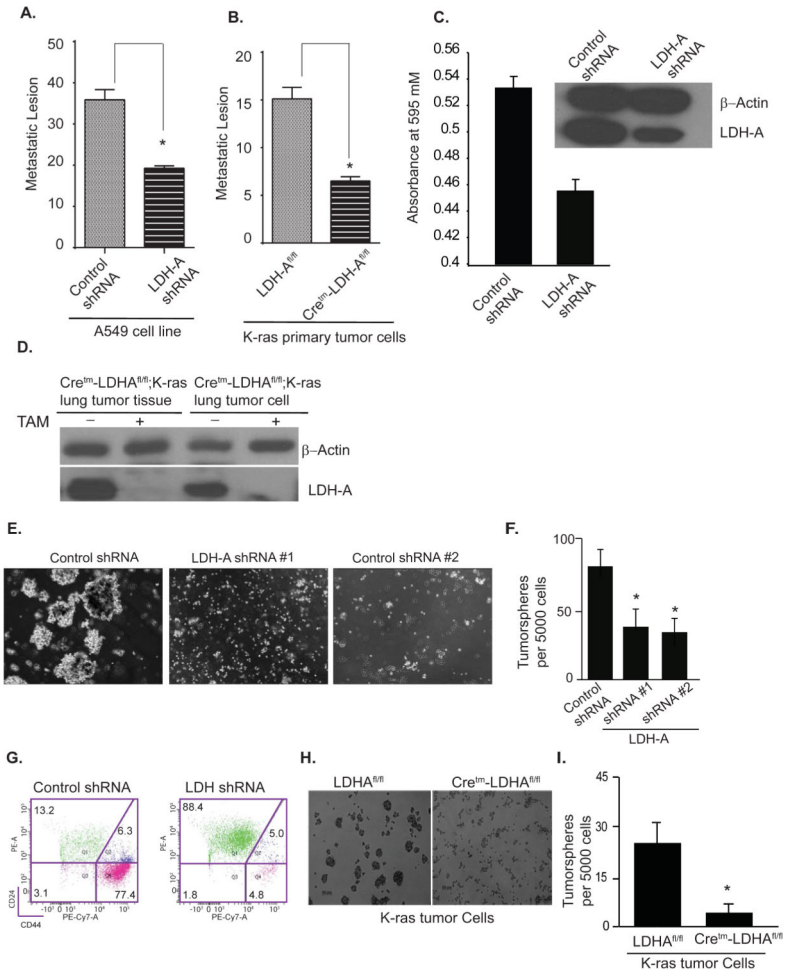

Fig. 4. *LDH-A* knockdown results in reduction of oncogenic *K-RAS*-induced cancer stem cells

Top Panel: Cancer-initiating cells within oncogenic *K-RAS*-expressing tumors are susceptible to *LDH-A* abrogation. (**A**) Cancer-initiating lesions from lungs of syngeneic mice (n=5) that were injected via tail vein with A549 cells expressing either control shRNA or *LDH-A* shRNA. Cancer-initiating lesions in (A) and (B) were scored after 24 days. (**B**) Cancer-initiating lesions from lungs of syngeneic mice (n=5) that were injected via tail vein with isolated tumor cells from tamoxifen-treated Cre^{tm}-*LDH-A*$^{fl/fl}$;*K-RAS* (n=3) or *LDH-A*$^{fl/fl}$;*K-RAS* (n=2) mice. Data is expressed as ± SEM (**=p < 0.01). (**C**) *In vitro* matrigel invasion assay with A549 cells expressing either control shRNA or *LDH-A* shRNA. Absorbance at 595 nm reflects the number of migrated cells. (**D**) Western immunoblotting for *LDH-A* and beta-actin of cells used in *in vitro* invasion and *in vivo* cancer initiation assays.

Bottom Panel: Stem cell populations within oncogenic ras-expressing cell lines are reduced by *LDH-A* shRNA. (**E**) A549 human NSCLC cells expressing control shRNA or two different *LDH-A* shRNAs were analyzed in tumorsphere formation assay and (**F**) Quantification of the results expressed as mean ± SD (*=p < 0.05) (**G**) FACS analysis of stem cell populations using CD44 and CD24 antibodies in Ras-transformed HMLE (HMLER) and shRNA-*LDH-A*-HMLER. (**H**) Tumorsphere formation assay using tumor

cells isolated from Cre^{tm}-*LDH-A*$^{fl/fl}$;*K-RAS* or *LDH-A*$^{fl/fl}$;*K-RAS* mice and (**I**) Graphical quantification of the results expressed as mean ± SD (*=p <0.05).

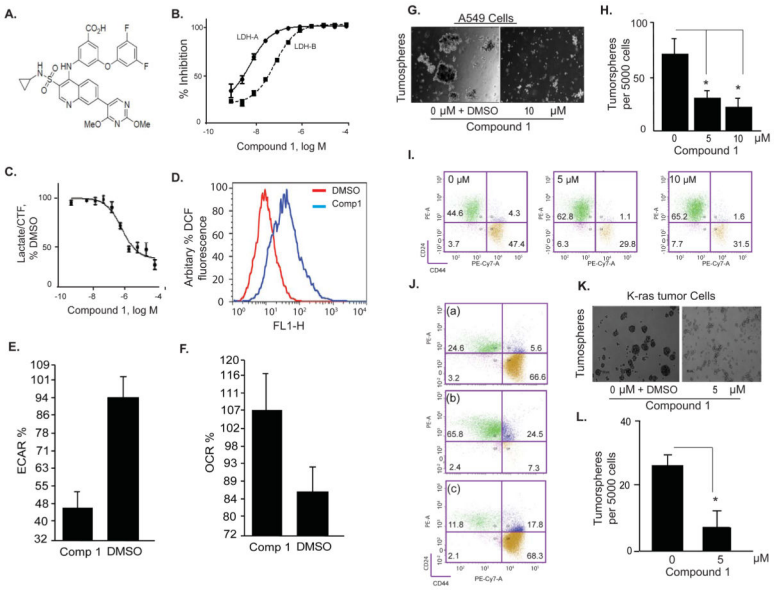

Fig. 5. Small molecule *LDH-A* inhibitor reduces the number of Ras-induced tumor stem cells

Left Panel: (**A**) Chemical structure of the Compound 1. (**B**) Compound 1 inhibits activity of recombinant human *LDH-A* (IC_{50}=4.8±1.1 nM) and LDH-B (IC_{50}=53.1±0.9 nM) enzymes. The signal obtained in absence of LDH was set as 100% inhibition and the signal obtained in absence of Compound 1 was set as 0% inhibition (DMSO control, not included on the graphs). Data are means ± SD of two readings, representative of 6 independent experiments. (**C**) Compound 1 inhibits lactate production in HepG2 human hepatocellular carcinoma cells. Lactate concentration was normalized to cell viability assessed by CellTiter-Fluor™ assay (CTF), and the lactate/CTF ratio obtained in DMSO-treated cells was set at 100%. (**D**) Compound 1 (10 μM) increases ROS activity in A549 cells as measured by DCF fluorescence (representative of two independent experiments). (**E**) Compound 1 (10 μM) increases oxygen consumption rate (OCR) and (**F**) decreased extracellular acidification rate (ECAR) in A549 cells. XF-24 seahorse cell analyzer was used to obtain the data (means ± SD of n=2).

Right Panel: (**G & H**) Tumorsphere formation assay with A549 cells using vehicle control or 10 μM Compound 1 with graphical quantitation of the results expressed as mean ± SD (*=p< 0.05). (**I**) FACS analysis using CD44 and CD24 antibodies for stem cell population in ras-transformed HMLE (HMLER) treated with 0, 5 and 10 μM Compound 1 for 30 hours. (**J**) Decrease in the stem cell population in HMLER by compound1 treatment is specific as shows that CD24/44 positive cells re-appear after withdrawal of the inhibitor (**a**) plated in absence of compound 1, (**b**) switched to media containing compound 1 for 24 hours, and (**c**), switched back to media without compound 1 for additional 24 hours. (**K & L**) Tumorsphere formation assay with tumor cells isolated from *LDH-A*$^{fl/fl}$;*K-RAS* mice treated with DMSO or 5 μM Compound 1, with graphical quantitation of results expressed as mean +/SD ($p < 0.05$).

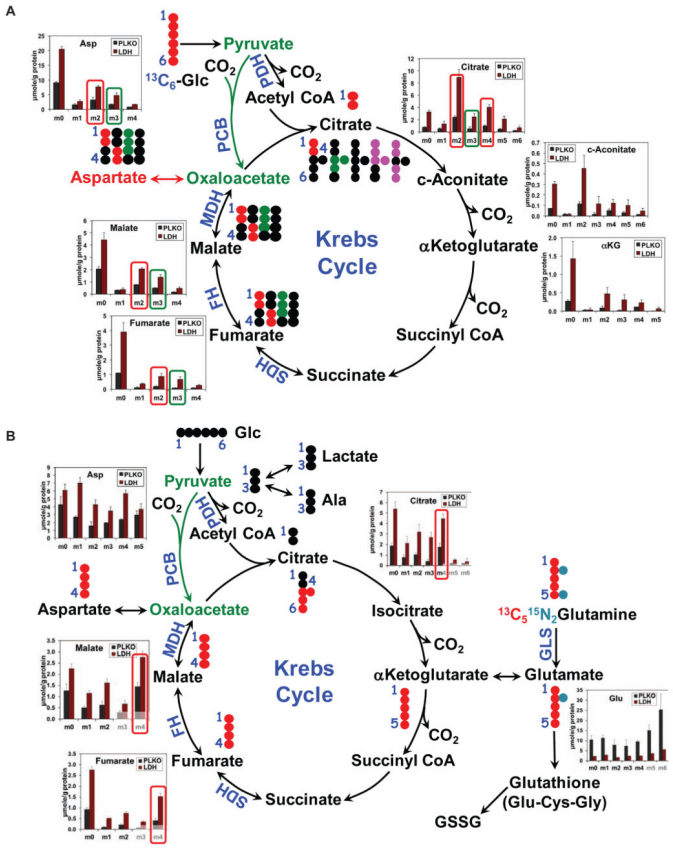

Fig. 6. Enhanced utilization of labeled glucose and glutamine via the Krebs cycle in *LDH-A* suppressed A549 cells

(**A & B**) A549 cells transduced with an empty vector (PLKO) or shRNA targeting *LDH-A* (LDH) were grown in $^{13}C_6$-glucose (**A**) or $^{13}C_5$,$^{15}N_2$-Gln (**B**) tracers for 24 h, as described in Methods. The polar extracts were analyzed by GC-MS for the distribution of various ^{13}C isotopologues (same metabolites with different numbers of ^{13}C atoms) of the Krebs cycle metabolites. Also shown in panels **A** and **B** are the atom-resolved Krebs cycle tracings with each respective tracer. The m2 ($^{13}C_2$) or m4 ($^{13}C_4$) isotopologues derived from either tracer via the Krebs cycle without input from pyruvate carboxylation (PC) are denoted with red rectangles while the m3 ($^{13}C_3$) isotopologues derived from $^{13}C_6$-glucose via PC are highlighted with green rectangles. Metabolite concentrations are means ± SD of two or three replicates. Solid and dashed arrows: single and multiple step reactions; single- and double-headed arrows: irreversible and reversible reactions, respectively; αKG: αketoglutarate; ●: ^{12}C; ●, ●: ^{13}C in the first and second turn without PC input; ●: ^{13}C with PC input.

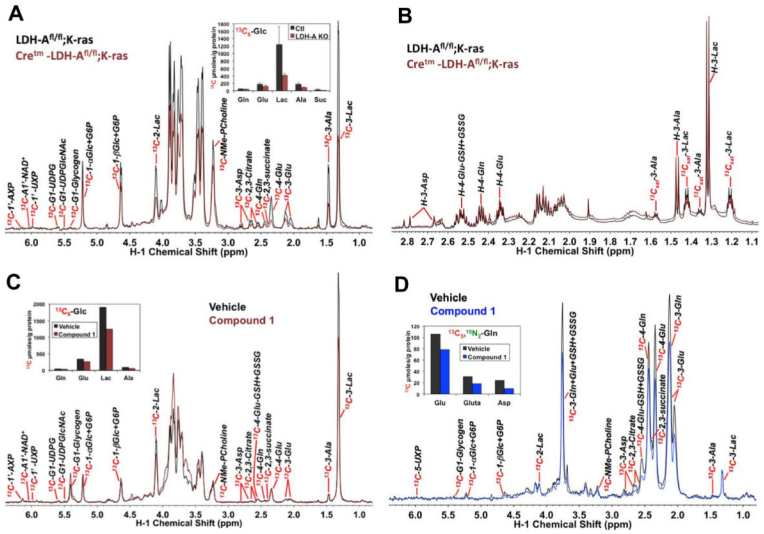

Fig. 7. LDH-A suppression in Cre^{tm}-*LDH-A*$^{fl/fl}$;*K-RAS*, mouse lung tumors and its pharmacological inhibition in primary human lung tumor tissue blocked glucose oxidation via glycolysis without activating the Krebs cycle

(**Top panel**) Four each *LDH-A*$^{fl/fl}$;*K-RAS* (Ctl) and Cre^{tm}-*LDH-A*$^{fl/fl}$;*K-RAS* (LDH-A KO) mice were tail vein injected with 20 mg of $^{13}C_6$-glucose in sterile PBS 3 times at 15 minute intervals prior to dissection for lung tumor tissues (one of the LDH-A KO mice had insufficient tissue for metabolite analysis). Polar metabolites were extracted from frozen pulverized tissue powder and analyzed by 1D ^{1}H and ^{1}H-{^{13}C} HSQC NMR as described for Warburg slices in Methods. (**A**) Displays the HSQC spectra for one pair of control versus LDH-A knockdown mouse tumors, where the intensity of each assigned metabolite ^{1}H signal reflect the ^{13}C abundance of the attached carbon. Also shown is the average content (mean±SE) of selected ^{13}C-labeled glycolytic and Krebs cycle metabolites (as ^{13}C μmole/g protein) obtained from the HSQC data (4 each for Ctl and LDH-A KO). ^{13}C-metabolites were quantified from the peak areas of respective HSQC resonances using the ^{13}C-3-Lac resonance as a calibrator. The ^{13}C abundance of 3-Lac was obtained from the ^{1}H NMR spectra as in (**B**) calibrated against the DSS standard. Lac: lactate; NMe-PCholine: N-methyl protons of phosphocholine; Glc: glucose; G6P: glucose-6-phosphate; UDP-GlcNAc: UDP-N-acetylglucosamine; UXP: uracil nucleotides; AXP: adenine nucleotides. LDH-A KO induced reduced production of ^{13}C-lactate from $^{13}C_6$-glucose, which is consistent with decreased glycolytic flow while it also elicited attenuated synthesis of ^{13}C-Ala, -Glu, -succinate, -citrate, and –Asp but this attenuation did not reach statistical significance (cf. Fig. S4). Suffice to say, Krebs cycle activity was not activated by LDH-A suppression. (**B**) Shows the ^{1}H spectrum of one of the five pairs of tumors. $^{13}C_{sat}$-3-Lac: the ^{13}C satellite peaks of the H3 of lactate, the pattern of which indicate fully ^{13}C labeled lactate; GSH+GSSG: reduced and oxidized glutathiones. Reduced production of ^{13}C-lactate and -Ala with little changes in the levels of the unlabeled counterparts is evident.

(**Bottom panel**) Two tissue slices were procured from one resected human NSCLC tumor, each treated with $^{13}C_6$-glucose and $^{13}C_5$,$^{15}N_2$-glutamine, and processed as described in Materials and Methods. (**C** and **D**) display respectively the 1D ^{1}H-{^{13}C} HSQC spectra of $^{13}C_6$-glucose and $^{13}C_5$,$^{15}N_2$-glutamine treated slices with or without LDH-A inhibitor (10

μM Compound 1). Also shown is the content of selected ^{13}C-labeled glycolytic and Krebs cycle metabolites (as ^{13}C μmole/g protein, determined as in (**A**)) obtained from the HSQC data. LDH-A inhibitor-induced reduction in ^{13}C-lactate production from $^{13}C_6$-glucose is evident in (**C**) while decreased synthesis of Krebs cycle metabolites (succinate, citrate, and Asp) and glutathiones from $^{13}C_5$,$^{15}N_2$-glutamine in response to LDH-A inhibition is shown in (**D**). Also clear from (**D**) is the lack of change in ^{13}C-lactate production from $^{13}C_5$,$^{15}N_2$-glutamine with LDH-A inhibition.